Spin observables in elastic proton scattering from polarized ^{3}He

E.J. Brash,* O. Häusser, W.J. Cummings, and M. Bahrami
Simon Fraser University, Burnaby, British Columbia, Canada V5A 1S6

P.P.J. Delheij, R.S. Henderson, M.C. Vetterli, and D.M. Whittal†
TRIUMF, 4004 Wesbrook Mall, Vancouver, British Columbia, Canada V6T 2A3

B. Larson
Ohio University, Athens, Ohio 45701

R.H. Landau and T. Mefford
Oregon State University, Corvallis, Oregon 97331

L. Ray
University of Texas at Austin, Austin, Texas 78712
(Received 14 February 1995)

We have measured the absolute cross section $\sigma(\theta)$ and complete sets of spin observables A_{00ij} in ^{3}He(p,p) elastic scattering at energies of 200 and 500 MeV. The observables depend on linear combinations of six complex scattering amplitudes for the p-^{3}He system and provide a severe test of current reaction models. The in-scattering plane observables (A_{00mm}, A_{00ll}, A_{00lm}, and A_{00ml}) are all in quantitative disagreement with fully microscopic nonrelativistic optical model calculations and nonrelativistic distorted wave Born approximation calculations.

PACS number(s): 25.10.+s, 24.70.+s, 25.40.Cm, 27.10.+h

I. INTRODUCTION

It has been recognized for many years that the N-N force is highly spin dependent. For example, data from pp scattering at 212 MeV [1] show conclusively that inclusion of the spin-orbit component of the nuclear force is crucial in describing the measured polarization observables.

It is also well known that it is possible to use nucleon-nucleus scattering as a probe of the spin structure of nuclei since target-related observables are extremely sensitive to small spin-dependent parts of the target wave function. It is this sensitivity that makes these spin observable data such a severe test of theoretical models. In addition, one can gain information about the nucleon-nucleus reaction mechanism, the spin dependence of the nucleon-nucleon interaction in the nuclear medium, and the off-shell behavior of the N-N amplitudes.

As a first step, spin effects in nucleon-deuteron scattering have been investigated in some detail. Recent full three-body calculations of n-d elastic scattering spin observables [2] are in good agreement with the available experimental p-d scattering data [3] (confirming that Coulomb effects are indeed small at the energies considered), and the observables are seen to be sensitive to small changes in the spin component of the N-N interaction. To extend the study of nuclear spin dependent effects to the $A = 3$ system, a high pressure polarized ^{3}He gas target has been developed, and this target has been used to measure spin observables and absolute cross sections in elastic scattering of polarized protons from polarized ^{3}He.

There are several factors which make ^{3}He an excellent choice as a nuclear target for the measurement of target-related spin dependent effects. The relative size of these effects is larger for ^{3}He than for any other dense nucleus ($A > 2$). For example, recent measurements of analyzing powers in elastic pion scattering [4–6] have shown that the asymmetries observed in the ^{3}He system are much larger than in either the ^{13}C or ^{15}N systems. Also, the availability of Faddeev calculations of the ^{3}He ground state wave function make it an attractive target from a theoretical standpoint. In addition, the predicted approximate alignment of the spin of the odd neutron with the ^{3}He spin indicates that one may be able to use polarized ^{3}He as a substitute for a polarized neutron target and hence measure properties of the fundamental N-N scattering system.

When studying nuclear spin effects, there are reasons why one expects the measured spin observables to differ from the free N-N values. The Fermi motion of the nucleons within the nucleus will result in an average of N-N observables over different energies and angles. Also, the nuclear response function may introduce a dependence of the observables on the energy transfer because the resid-

*Present address: Rutgers University, Box 849, Piscataway, NJ 08855.
†Permanent address: National Accelerator Centre, Faure, 7131, South Africa.

ual N-N interaction is either attractive or repulsive for different spin-isospin channels. Thus it is necessary to confront theory with as many observables as possible in order to separate out these various effects.

To this end, we have made measurements of absolute cross sections and the complete set of spin observables A_{00ij} in the scattering of polarized protons from polarized ^{3}He at incident proton energies of 200 and 500 MeV. Here, ij are the parity allowed combinations of normal, sideways, and longitudinal polarizations of both beam and target.

In the second section of this paper we outline two sets of calculations which predict the spin observables for the ^{3}He(p,p) reaction. Both calculations are optical model reaction theories which utilize the impulse approximation. The first calculation, by Landau *et al.* [7], uses the nonrelativistic "factorized" form for the momentum space optical potential wherein different components of the N-N t matrix are multiplied by the appropriate nuclear form factors. The second calculation, by Ray *et al.* [8], uses distorted waves calculated using the Schrödinger equivalent potential from a phenomenological Dirac optical potential in a nonrelativisitic distorted wave Born approximation (DWBA) calculation.

The theoretical section will be followed by a description of the experimental details and data analysis techniques. Finally, the results will be discussed.

II. OPTICAL MODEL CALCULATIONS OF $\vec{p}$-$^3\vec{\text{H}}$E ELASTIC SCATTERING

The $\vec{p}$-$^3\vec{\text{H}}$e system is a spin $\frac{1}{2}\bigotimes\frac{1}{2}$ system and therefore has many similarities to the elementary N-N system. In particular, the N-N and p-^{3}He T matrices or scattering amplitudes have the same spin-space structure [9,10],

$$\begin{aligned} T = [&(a+b)+(a-b)\vec{\sigma}_p\cdot\hat{\mathbf{n}}\vec{\sigma}_2\cdot\hat{\mathbf{n}} \\ &+(c+d)\vec{\sigma}_p\cdot\hat{\mathbf{m}}\vec{\sigma}_2\cdot\hat{\mathbf{m}}+(c-d)\vec{\sigma}_p\cdot\hat{\mathbf{l}}\vec{\sigma}_2\cdot\hat{\mathbf{l}} \\ &+e(\vec{\sigma}_p+\vec{\sigma}_2)\cdot\hat{\mathbf{n}}+f(\vec{\sigma}_p-\vec{\sigma}_2)\cdot\hat{\mathbf{n}}]/2, \end{aligned} \tag{1}$$

where $\vec{\sigma}_p$ refers to the spin of the projectile (proton) and $\vec{\sigma}_2$ to that of the target. In the N-N system, the f amplitude is exactly zero due to the fact that target and projectile are identical particles (if charge independence is assumed [7]).

Assuming that the strong interaction conserves parity and time reversal, the spin-dependent cross section for scattering of a spin-$\frac{1}{2}$ projectile by a spin-$\frac{1}{2}$ target is given by [11]

$$\begin{aligned} \sigma = \sigma_0[1 &+P_b(\hat{N})A_{00N0}+P_t(\hat{N})A_{000N} \\ &+P_b(\hat{N})P_t(\hat{N})A_{00NN}+P_b(\hat{L})P_t(\hat{L})A_{00LL} \\ &+P_b(\hat{S})P_t(\hat{S})A_{00SS}+P_b(\hat{S})P_t(\hat{L})A_{00SL} \\ &+P_b(\hat{L})P_t(\hat{S})A_{00LS}], \end{aligned} \tag{2}$$

where σ_0 is the spin-independent cross section, and P_b and P_t are the beam and target polarizations, respectively. The unit vectors $\hat{N}$, $\hat{S}$, and $\hat{L}$ define the normal (perpendicular to the scattering plane), sideways (in the scattering plane and perpendicular to the beam direction), and longitudinal (along the beam direction) directions. It is clear from the form of Eq. (2) that by choosing particular directions for the beam and target polarizations, one becomes sensitive to particular observables.

The center-of-mass coordinate system is related to the laboratory coordinate system according to the transformation

$$\begin{bmatrix} m \\ n \\ l \end{bmatrix} = \begin{bmatrix} \cos(\theta/2) & 0 & -\sin(\theta/2) \\ 0 & 1 & 0 \\ \sin(\theta/2) & 0 & \cos(\theta/2) \end{bmatrix} \begin{bmatrix} S \\ N \\ L \end{bmatrix}, \tag{3}$$

where θ is the scattering angle in the center-of-mass system. The center-of-mass observables may be derived from linear combinations of the lab observables, for example,

$$\begin{aligned} A_{00lm} = &\sin(\theta/2)\cos(\theta/2)(A_{00SS}-A_{00LL}) \\ &-\sin^2(\theta/2)A_{00SL}+\cos^2(\theta/2)A_{00LS}. \end{aligned} \tag{4}$$

Notice that the normal observables are the same in both the lab and center-of-mass systems.

A. Fully microscopic nonrelativistic optical potential calculation

At intermediate energies it is expected to be a good approximation to use a simple product or "factorized" form for the momentum space optical potential [7] wherein the different components of the NN t matrix are multiplied by the appropriate nuclear form factors. Since the matter and spin form factors are quite different, the effective "shape" of the optical potential reflects both. Since the potential includes the finite range of the NN force, off-shell kinematics, and recoil and binding corrections, it is inherently nonlocal and has no simple coordinate-space form. The first order optical potential used in [7] is

$$\begin{aligned} U(\vec{k}'|\vec{k}) \simeq U^1(\vec{k}'|\vec{k}) &= \langle\psi_A|\,t^{pN}\,|\psi_A\rangle \\ &\approx N\{t^{pn}_{A+B}\rho^n_{\rm mt}(q)+[t^{pn}_{A-B}\vec{\sigma}_p\cdot\hat{\mathbf{n}}\vec{\sigma}_n\cdot\hat{\mathbf{n}}+t^{pn}_E\vec{\sigma}_n\cdot\hat{\mathbf{n}}+t^{pn}_{C+D}\vec{\sigma}_p\cdot\hat{\mathbf{m}}\vec{\sigma}_n\cdot\hat{\mathbf{m}}+t^{pn}_{C-D}\vec{\sigma}_p\cdot\hat{\mathbf{l}}\vec{\sigma}_n\cdot\hat{\mathbf{l}} \\ &\quad +t^{pn}_{CD}(\vec{\sigma}_p\cdot\hat{\mathbf{m}}\vec{\sigma}_n\cdot\hat{\mathbf{l}}+\vec{\sigma}_p\cdot\hat{\mathbf{l}}\vec{\sigma}_n\cdot\hat{\mathbf{m}})]\rho^n_{\rm sp}(q)+t^{pn}_E\vec{\sigma}_p\cdot\hat{\mathbf{n}}\rho^n_{\rm mt}(q)\}+\left\{\frac{N\to Z}{n\to p}\right\}, \end{aligned} \tag{5}$$

where $\rho^n_{\rm mt}$ and $\rho^n_{\rm sp}$ are the matter and spin densities for neutrons in ^{3}He. The directions $\hat{\mathbf{n}}$, $\hat{\mathbf{m}}$, and $\hat{\mathbf{l}}$ are defined in terms of the momentum vectors of the incident proton ($\mathbf{k}$) and the scattered proton ($\mathbf{k}$) by

$$\hat{\mathbf{n}} = \frac{\mathbf{k}\times\mathbf{k}'}{|\mathbf{k}\times\mathbf{k}'|}, \quad \hat{\mathbf{m}} = \frac{\mathbf{k}'-\mathbf{k}}{|\mathbf{k}'-\mathbf{k}|}, \quad \hat{\mathbf{l}} = \frac{\mathbf{k}+\mathbf{k}'}{|\mathbf{k}+\mathbf{k}'|}, \tag{6}$$

so that $\hat{\mathbf{n}}$ is normal to the scattering plane. The t matrices $t^{pn}_{A+B}\ldots$ differ from the scattering amplitudes of Eq. (1) by kinematic factors only. The spin and matter densities for protons and neutrons in ^{3}He are derived from the Faddeev wave functions of Ref. [12]. While not immediately obvious from the form of Eq. (5), both the e and f amplitudes of Eq. (1) are contained in it. A slight restructuring of the t_E terms yields the e and f parts of the optical potential

$$U_e = \frac{1}{2}\left[Nt^{pn}_E(\rho^n_{\rm mt}+\rho^n_{\rm sp}) + Zt^{pp}_E(\rho^p_{\rm mt}+\rho^p_{\rm sp})\right](\sigma^p+\sigma^2) \tag{7}$$

and

$$U_f = \frac{1}{2}\left[Nt^{pn}_E(\rho^n_{\rm mt}-\rho^n_{\rm sp}) + Zt^{pp}_E(\rho^p_{\rm mt}-\rho^p_{\rm sp})\right](\sigma^p-\sigma^2)\ . \tag{8}$$

Since the spin and matter densities are not equal for both neutrons and protons in ^{3}He, one expects a nonvanishing f amplitude.

The Lippmann-Schwinger equation to be solved using the above potential is

$$T^{JS}_{ll'}(k',k) = U^{JS}_{ll'}(k',k) + \frac{2}{\pi}\sum_L \int_0^\infty p^2 dp \frac{U^{JS}_{lL}(k',p)T^{JS}_{Ll'}(p,k)}{E(k_o)-E(p)+i\epsilon}, \tag{9}$$

where $E(k_o) = E_p(k_o) + E_A(k_o)$ is the total relativistic energy of the projectile (p) and target (A) with c.m. momentum k_o. A proper development of the f term in the optical potential requires coupling of the singlet and triplet ($S=0$ and $S=1$) partial waves [7] which is forbidden in the NN system because of the generalized Pauli exclusion principle.

The dependence of the center-of-mass spin observables on the six complex amplitudes of Eq. (1) is [7]

$$\sigma = (|a|^2+|b|^2+|c|^2+|d|^2+|e|^2+|f|^2)/2, \tag{10}$$
$$A_{00n0} = \mathrm{Re}(a^*e+b^*f)/\sigma, \tag{11}$$
$$A_{000n} = \mathrm{Re}(a^*e-b^*f)/\sigma, \tag{12}$$
$$A_{00nn} = (|a|^2-|b|^2-|c|^2+|d|^2+|e|^2-|f|^2)/2\sigma, \tag{13}$$
$$A_{00mm} = \mathrm{Re}(a^*d+b^*c)/\sigma, \tag{14}$$
$$A_{00lm} = -\mathrm{Im}(d^*e+c^*f)/\sigma, \tag{15}$$
$$A_{00ml} = -\mathrm{Im}(d^*e-c^*f)/\sigma, \tag{16}$$
$$A_{00ll} = -\mathrm{Re}(a^*d-b^*c)/\sigma. \tag{17}$$

B. Nonrelativistic DWBA calculation

Nonrelativistic DWBA calculations for p+^{3}He elastic scattering were done using a formalism which was originally developed for relativistic impulse approximation calculations of spin observables in the p-^{13}C system (see Ref. [8]). The formalism in this reference is the relativistic DWBA using four-component Dirac wave functions. The NN t matrix, which is cast into a Lorentz invariant form involving the five terms: scalar, vector, pseudoscalar, axial vector, and tensor, is

$$t_{pi} = F_S + F_P\gamma^5_p\gamma^5_i + F_V\gamma^\mu_p\gamma_{i\mu} + F_A\gamma^5_p\gamma^\mu_p\gamma^5_i\gamma_{i\mu} + F_T\sigma^{\mu\nu}_p\sigma_{i\mu\nu}\ , \tag{18}$$

where the subscript p indicates the incident proton and the subscript i indicates a particular target nucleon.

For the case of p-^{3}He elastic scattering, Ray *et al.* use a *nonrelativistic* DWBA using the formalism of Ref. [8]. To use this formalism to do a nonrelativistic calculation, several assumptions are made. The ^{3}He ground state wave function used in these calculations is that of 3 nucleons in the $1s_{1/2}$ orbital. The wave functions are adjusted to fit the total ^{3}He magnetic form factor of Ref. [12]. Since the momentum transfers involved are relatively small, the lower components of both the distorted waves and the $2s_{1/2}$ ^{3}He wave function are set to their free particle values, i.e.,

$$\psi_L = \frac{\sigma\cdot k}{E+m}\psi_U\ . \tag{19}$$

As well, the proton mass is replaced with the reduced total energy in the p-^{3}He c.m. system.

For the p-^{13}C calculation of Ref. [8], the distorted waves were calculated from an optical potential corresponding to the ^{12}C core. Such an optical potential, since it describes a spin-zero nucleus, contains only scalar and timelike vector pieces. Hence, for the p-^{3}He calculations, the distorted waves were calculated using the scalar and timelike vector parts of the full p-^{3}He Dirac phenomenological optical potential fit to the differential cross section and analyzing power data. The valence (or Born) part of the potential includes the pseudoscalar, spacelike vector, axial vector, and tensor parts of the p-neutron interaction.

III. EXPERIMENT

This experiment was conducted in the proton hall of the TRI-University Meson Facility (TRIUMF). Proton beams of greater than 80% polarization in the normal ($\hat{\mathbf{n}}$) direction are produced by the Lamb shift ion source and accelerated in the TRIUMF cyclotron to energies between 200 and 515 MeV depending on the radius of beam extraction. Beamline 4B (BL4B) was used to transport the beam to the pivot of the medium resolution spectrometer (MRS) where it was incident on a polarized ^{3}He target. The MRS facility was then used to analyze the momentum of the scattered protons and provide traceback to the target to eliminate protons originating from the glass walls and endcaps of the ^{3}He target cell.

The sideways ($\hat{\mathbf{s}}$) and longitudinal ($\hat{\mathbf{l}}$) polarized proton beams were produced using two superconducting spin

precession solenoids which are alternated with two dipole bending magnets. The normal function of the bending magnets is to direct the beam into beamline 4B. In this experiment they also serve to precess the beam polarization in the horizontal plane. This is necessary for production of $\hat{\mathbf{l}}$ type beams. With this combination of elements, the polarization of the proton beam that exits the cyclotron can be rotated from $\hat{\mathbf{n}}$ to either $\hat{\mathbf{s}}$ or $\hat{\mathbf{l}}$. The beam polarization was measured in the $\hat{\mathbf{n}}$ and $\hat{\mathbf{s}}$ directions using the TRIUMF in-beam-polarimeter (IBP). The IBP was also calibrated against a Faraday cup and provided the absolute normalization of the beam charge.

The IBP consists of a thin CH_2 target and four scintillator telescopes; one on either side and above and below the CH_2 target. The telescopes measure the number of protons scattered to the left (N_{left}), to the right (N_{right}), to the top (N_{top}), and to the bottom (N_{bot}) at a 17° lab angle in coincidence with the corresponding recoil proton scattered to the opposite side of the beam. Accidental coincidences are determined and subtracted to obtain the true number of scattered protons. The analyzing power of CH_2 is large at this angle but varies with energy from 0.28 at 200 MeV to 0.47 at 500 MeV. The beam polarization in the sideways or normal directions are then determined from the expression

$$P\underset{n}{s} = \epsilon\underset{n}{s}/A_y,$$

where

$$\epsilon_s = \frac{N_{\text{top}} - N_{\text{bot}}}{N_{\text{top}} + N_{\text{bot}}}, \quad \epsilon_n = \frac{N_{\text{left}} - N_{\text{right}}}{N_{\text{left}} + N_{\text{right}}} \tag{20}$$

is the measured asymmetry. For longitudinally polarized beam, the beam polarization was taken to be the average value of previous and subsequent runs with the beam polarized in the sideways direction.

A. Medium resolution spectrometer

The medium resolution spectrometer (MRS) has been discussed extensively elsewhere [13]; therefore only a brief description will be given here. The MRS is depicted schematically in Fig. 1. The MRS consists of a quadrupole and dipole magnet combination. The dipole magnet has a central bend angle of 60° in the vertical direction and a momentum acceptance of $\Delta P/P \approx \pm$ 7% for particle momenta up to about 1.5 GeV/c.

Ray tracing through the spectrometer is provided by two sets of drift chambers containing two orthogonal sets of two wire planes each located in front of the MRS quadrupole (FEC's) and two sets of vertical drift chambers (VDC's) with two wire planes each located just above the focal plane of the MRS. The FEC coordinates are used to (1) define the angular acceptance of the MRS, (2) correct for aberrations in the spectrometer, and (3) provide traceback to the target to eliminate events which originated in the endcaps of the target cell. Each FEC plane consists of 16 alternating anode and cathode wire pairs spanning 8 cm. There are two wire planes in each

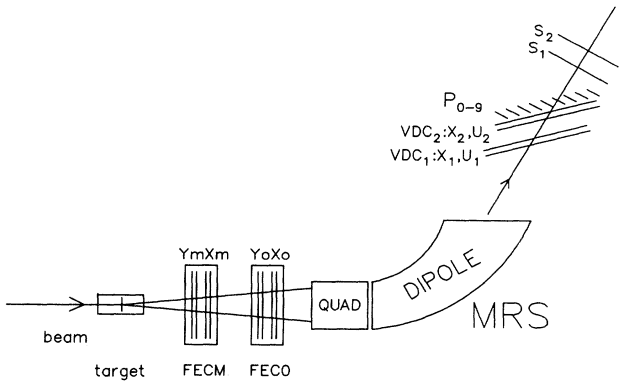

FIG. 1. The medium resolution spectrometer (MRS) system.

direction labeled XM, XM', YM, and YM' for the first chamber and $X0$, $Y0$, etc. for the second. The primed planes are offset from the unprimed planes by one half of an anode spacing to remove the "left-right" ambiguity. The position of the struck wire in the primed plane indicates whether the proton passed to the left or to the right of the struck wire in the unprimed plane. This arrangement also allows interpolation using drift times (with an accuracy of $\sim \pm 0.5$ mm) that would otherwise not be possible. The FEC's also constituted part of the MRS trigger.

Each VDC chamber contains two crossed wire planes, one in the X (bend) direction and one at 30° to X. These are later transformed into X and Y. Readout of the wire chamber data is handled by a Lecroy 4290 drift chamber control system. For a particular VDC track at least three wires are required for a valid hit. From these data the X and Y coordinates are calculated with a resolution of 150 μm.

B. TRIUMF polarized ^{3}He target

Polarized ^{3}He target cells produced at TRIUMF have been designed to meet the requirements of proton and pion scattering experiments. The general features of the TRIUMF optically pumped polarized ^{3}He target have been described elsewhere (see Ref. [14]) and will only be described very briefly here. In earlier experiments the target spin was reversed using the adiabatic fast passage (AFP) method. Since this method is time consuming and polarization losses of greater than 1% are common, the polarization was reversed at several hour intervals. For this experiment, an adiabatic spin rotator (ASR) was used and the spin was reversed every 10 minutes (see Ref. [15] for a detailed description of the ASR). This allowed sufficient time for one beam polarization cycle to be completed within each target polarization state. This will be described in more detail later.

For proton beam experiments where the beam diameter is approximately 2 mm, target cells of 17 mm outer diameter and 8 cm length (volume $\approx$ 17 cm^3) are adequate.

In this experiment, a cell of 9 atm pressure (2.4×10^{20}) atom/cm^3 was used. Since the useful length of the cell was only 5 cm the areal density was 1.2×10^{21} atom/cm^2 (6 mg/cm^2). Besides the ^{3}He, the cell contains a few mg of Rb alkali metal and $\approx$100 Torr of N_2 quench gas. The glass cell was mounted in an oven made of the polyimide VESPEL. Windows consisting of two layers of 25 μm kapton separated by an air gap of 6 mm were used to reduce heat loss and thermal gradients within the oven while contributing a minimal amount to the energy loss of the incident and scattered protons. The oven was operated at a temperature of 450 K to produce a Rb density of $\sim 4 \times 10^{14}$ cm^{-3}. About 8 W of circularly polarized photons (λ = 795.8 nm) were used to optically pump Rb via the $D1$ line.

The ^{3}He polarization produced by the Fermi contact hyperfine interaction during Rb-^{3}He spin exchange collisions was analyzed by adiabatic fast passage NMR. The NMR signal induced by the rotating ^{3}He magnetic moment was compared to that from a water sample of similar geometry to obtain an absolute value of the polarization. Measurement of the target polarization was performed at intervals of 4–6 hours. In an earlier experiment at TRIUMF [16], an independent check of the NMR method was developed. The new method is based on the special properties of the $^3\vec{\text{He}}(\vec{p},\pi^+)^4$He reaction and is sensitive only to ^{3}He in the beam interaction region. Parity conservation in the strong interaction, channel spins 1 and 0 for entrance and exit channels, and parity change in the reaction, imply the identities $A_{nn} = 1$ and $A_{no} = A_{on}$ for spin correlation parameter and beam- and target-related analyzing powers [11]. After determining the beam-related analyzing power A_{no} for 416 MeV polarized protons at a laboratory scattering angle of 28°, absolute ^{3}He polarizations were obtained to an accuracy of $\pm$0.02. The absolute ^{3}He polarization results from the reaction method were in good agreement with the AFP NMR measurements. The reaction method is more direct and less susceptible to systematic errors than NMR, but requires expensive accelerator time. The ^{3}He polarization results of the present work were obtained with the more readily available NMR method. Because of the weakness of the water signal, which is smaller than the ^{3}He signal by a factor of $(3.71 \times 10^4)pP$ where p and P are the ^{3}He pressure, in standard atmospheres, and polarization, respectively, and a significant temperature dependence in the induced NMR signal, a systematic uncertainty of $\Delta P_t/P_t$=0.05 has been adopted for the absolute ^{3}He polarization.

To provide sideways and longitudinal target polarizations, an adiabatic spin rotator was used. The ASR was also used to perform the spin reversals. The technique involves slowly rotating the magnetic holding field direction through 180 degrees while keeping the magnitude of the field approximately constant. The spin reversal was controlled by computer and required approximately 30 seconds to perform. This limitation came mainly from the speed at which the $\lambda/4$ plate could be rotated. The ASR apparatus consists of two perpendicular pairs of Helmholtz coils. One set provides a vertical field and the other a horizontal field. A schematic drawing of the apparatus is presented in Fig. 2. As shown in the figure, the optical pumping was performed in the sideways direction. The horizontal field coils could be manually rotated about the vertical axis by 90 degrees allowing the target polarization to be rotated from $\hat{\mathbf{s}}$ to $\hat{\mathbf{l}}$ with relative ease.

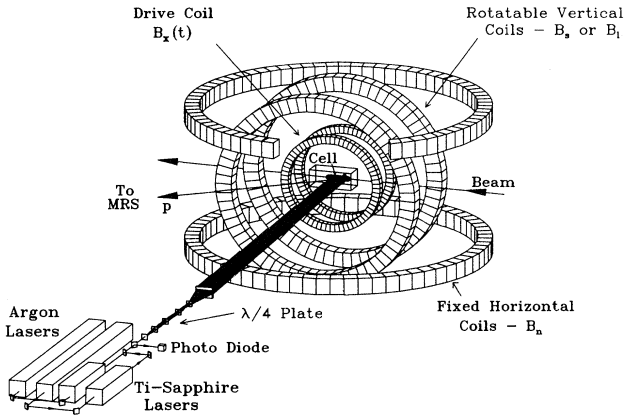

FIG. 2. The optical pumping apparatus and holding field system.

During a spin reversal the vertical field is ramped from 0 G to about 30 G and back to 0 G while the horizontal field is lowered from about 30 G through 0 G and up to 30 G in the opposite direction. The maximum of the vertical field is timed to coincide with the zero crossing of the horizontal field. Due to the technical difficulties involved with optical pumping in both the $\hat{\mathbf{s}}$ and $\hat{\mathbf{l}}$ directions we chose to pump in the $\hat{\mathbf{s}}$ direction only. The $\hat{\mathbf{l}}$ polarized data were accumulated while the ^{3}He polarization was allowed to decay at room temperature. Starting with sideways polarization, the target was pumped to its maximum value of 65%. Data were then accumulated for approximately 8 h in each target spin state. Since the inverse of the decay rate for our target cell at room temperature was about 40 h, only 20% of the polarization was lost during 8 hours of decay. The inverse of the optical pumping time constant is about 10 h therefore 8 hours of optical pumping at T = 450 K brought the polarization up to $>$ 90% of its maximum value. With this target polarization cycle, the polarization was maintained between 50 and 65% for the duration of the experiment.

Measurements were performed at 200 and 500 MeV incident proton energy. At 200 MeV an angular range of 24 to 73 degrees was covered while the angular range extended only up to 53 degrees for the 500 MeV data. The data are presented in Sec. V.

IV. DATA ANALYSIS

A. Data reduction

Several software cuts were made, in addition to the hardware requirements discussed previously, to extract a set of events from all of the accumulated data which

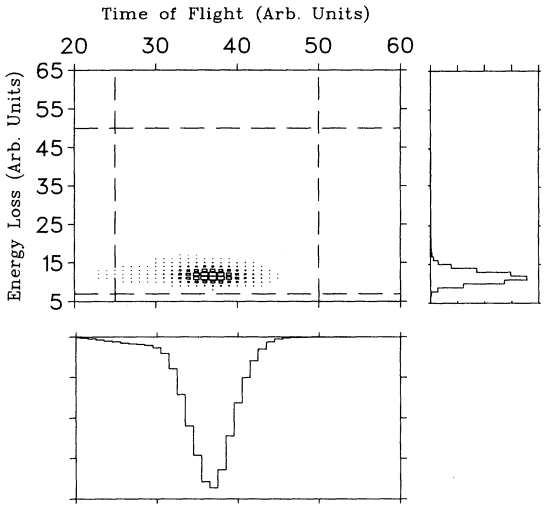

FIG. 3. Identification of protons in the MRS.

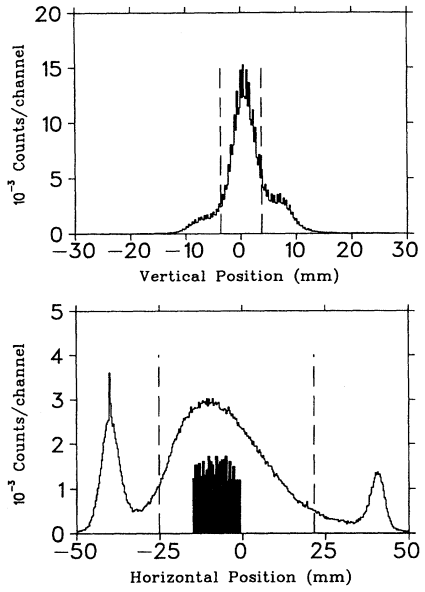

FIG. 4. Vertical and longitudinal ray tracing of protons in the MRS back to the target.

contained as few background events as possible. The following subsection describes these cuts in detail.

The energy deposit of particles in the MRS paddles along with the time of flight from the FEC's to these paddles was used in order to identify scattered protons (see Fig. 3). It is possible to clearly separate the scattered protons from other particles, especially protons from other beam bursts, which come 43 ns apart. This software cut rejected about 0.5% of the accumulated data. It was found that the average efficiency of the FEC's varied from 70% at the smallest angles to 82% at the larger angles. The average efficiency of the VDC's was about 92%. This resulted in an overall acceptance of 64–75% of the data base.

B. Background

As mentioned in the previous section, the major source of background in this experiment was events which originated from the glass cell entry and exit windows. The traceback spectra obtained using the FEC's in both the vertical and longitudinal (along the beam) directions are shown in Fig. 4. The vertical traceback spectrum shows that there is some interaction of the incoming proton beam with the side walls of the cell. However, these events were eliminated using the software cuts shown. The longitudinal spectrum shows the separation of glass events from ^{3}He events, along with the cuts used to eliminate glass events. The dashed lines in this spectrum indicate the cuts used for spin observable measurements. The solid spectrum is a typical spectrum for the absolute cross-section measurements. Here the solid angle of the MRS was 0.768 msr (32 mrad polar, 24 mrad azimuthal).

Another source of background comes from scattering off the N_2 quench gas in the target. The overlap of the nitrogen elastic peak with the ^{3}He elastic peak is minimal. As well, the inelastic background for nitrogen is both small and smoothly varying with missing energy. Thus the background from nitrogen scattering can be subtracted reliably from the ^{3}He elastic peak.

C. Identification of elastically scattered protons

After application of the previous particle identification and trajectory reconstruction software cuts, it was necessary to distinguish between protons which had scattered elastically from ^{3}He within the target and those which had scattered by some other process. In Fig. 5 is shown a typical spectrum of yield as a function of energy loss of the incident proton at a lab scattering angle of 27.5° and incident proton energy of 200 MeV. Kinematic calculations show that the elastic peak is expected at an energy loss of about 19.6 MeV when one takes into account the energy loss in the scattering as well as in the glass walls of the cell. The elastic peak is clearly visible in the figure and is well separated from inelastic events.

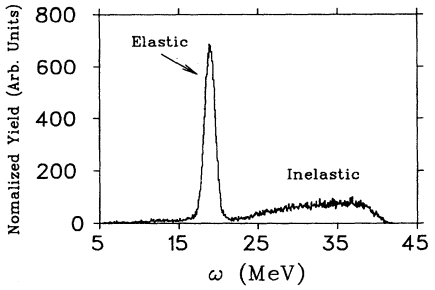

FIG. 5. Typical missing energy spectrum for protons elastically scattered from ^{3}He. The incident proton energy is 200 MeV and the laboratory scattering angle is 27.5°.

In the determination of raw yields, this peak was fitted over the energy loss region from 15 to 24 MeV with a Gaussian line shape together with a linear background fitting function.

D. Yield normalization factors

In this subsection, the correction factors needed to normalize yields from several different runs are discussed.

The differential cross section for the elastic scattering process can be written

$$\frac{d\sigma}{d\Omega} = \frac{N_{\rm scat} A}{N_{\rm inc} N_o \tau} \frac{1}{\Delta\Omega}, \tag{21}$$

where $N_{\rm inc}$ is the number of incident particles, A is the atomic weight of the target nuclei, N_o is Avogadro's number, τ is the areal density of the target, and $\Delta\Omega$ is the allowed solid angle for scattering which was determined by gates applied to the FEC coordinates. The areal density of the target is given by ρ/Δ_{ZI} where ρ is the ^{3}He density and Δ_{ZI} is the target length as defined by the software gates on the longitudinal traceback spectrum. The true number of scattered particles $N_{\rm scat}$ is determined from the measured yields $N_{\rm meas}$ by

$$N_{\rm scat} = \frac{N_{\rm meas}}{\rm lt \cdot \epsilon \cdot acc}, \tag{22}$$

where lt is the electronics live time, ϵ is the total detector efficiency, and acc is the MRS acceptance correction. As mentioned previously the electronics live time is given by the ratio of the number of random pulser events accepted by the acquisition system to the total number submitted. The live time varied between 65% and 75% over the course of the experiment. The yields were corrected for absolute MRS wire chamber efficiency, which was discussed in the previous chapter.

E. Extraction of spin observables

The spin dependent cross section for the $^3\vec{\rm He}(\vec{p},p)$ reaction has been given in Eq. (2). It should be noted that observables such as A_{00L0} and A_{00S0} are zero as a consequence of parity conservation of the strong interaction and therefore do not appear in Eq. (2). As an illustration of the method used for extraction of the spin observables we will now consider the situation of both the beam polarization and target polarization normal to the scattering plane. For measurements of the spin observables it is only necessary to consider the normalized yields rather than the absolute cross sections as these differ only by a constant, and this constant will cancel in the calculation of any particular observable. For the four possible spin combinations for beam and target, the following relations hold:

$$Y_{\uparrow\uparrow} = Y_0(1 + P^b_\uparrow A_{00N0} + P^t_\uparrow A_{000N} + P^b_\uparrow P^t_\uparrow A_{00NN}), \tag{23}$$

$$Y_{\uparrow\downarrow} = Y_0(1 + P^b_\uparrow A_{00N0} - P^t_\downarrow A_{000N} - P^b_\uparrow P^t_\downarrow A_{00NN}), \tag{24}$$

TABLE I. Extraction of spin observables and absolute cross sections.

Beam polarization	Target polarization	Quantity extracted
Normal	Normal	σ_0, A_{00N0}, A_{000N}, A_{00NN}
Sideways	Sideways	A_{00SS}
Sideways	Longitudinal	A_{00SL}
Longitudinal	Sideways	A_{00LS}
Longitudinal	Longitudinal	A_{00LL}

$$Y_{\downarrow\uparrow} = Y_0(1 - P^b_\downarrow A_{00N0} + P^t_\uparrow A_{000N} - P^b_\downarrow P^t_\uparrow A_{00NN}), \tag{25}$$

$$Y_{\downarrow\downarrow} = Y_0(1 - P^b_\downarrow A_{00N0} - P^t_\downarrow A_{000N} + P^b_\downarrow P^t_\downarrow A_{00NN}), \tag{26}$$

where Y_{bt} denotes the measured normalized yield for the respective spin states of beam and target. This set of equations was solved numerically using the CERN library software package MINUIT [17]. In the results shown in the Sec. V the error bars shown in the figures are statistical uncertainties. In the tables both the statistical uncertainty and a systematic uncertainty resulting from uncertainties in the beam and target polarizations (ΔP_b=1%,ΔP_t=5%) are given.

The spin observables and absolute cross sections were determined using the above procedure for the ^{3}He(p,p) reaction. In Table I are shown the various combinations of beam and target polarizations used and the quantity extracted. The results of these analyses are discussed in Sec. V.

V. RESULTS AND DISCUSSION

The first measurement of spin observables for the $^3\vec{\rm He}(\vec{p},p)$ reaction was carried out by Häusser *et al.* [18]. The cross section and beam related analyzing powers are fairly well reproduced by the calculations of Landau *et*

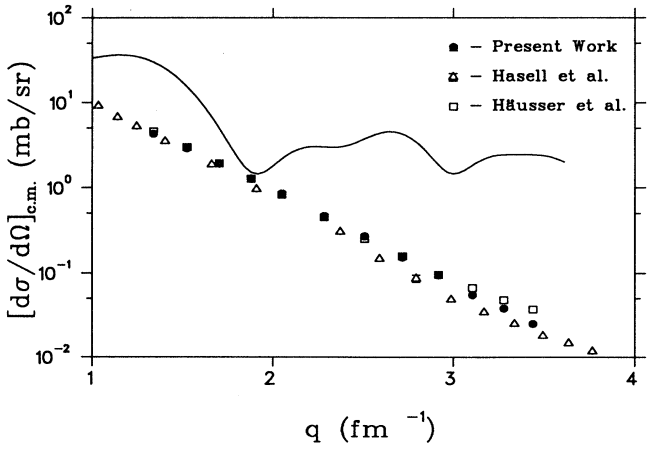

FIG. 6. Differential cross sections for the $^3\vec{\rm He}(\vec{p},p)$ reaction at 200 MeV. The solid line is the fully microscopic optical potential calculation of Ref. [7].

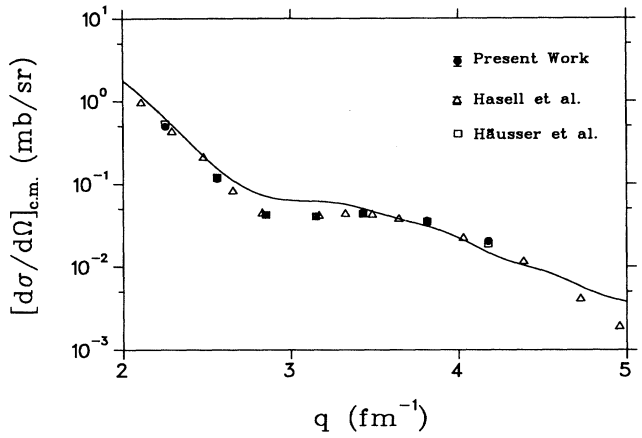

FIG. 7. Differential cross sections for the $^3\vec{\text{He}}(\vec{p},p)$ reaction at 500 MeV. The solid line is the fully microscopic optical potential calculation of Ref. [7].

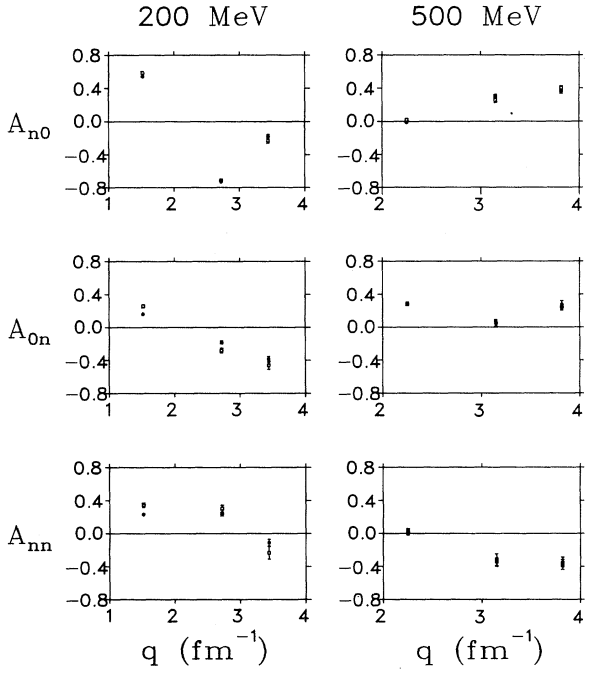

FIG. 8. Normal spin observables for the $^3\vec{\text{He}}(\vec{p},p)$ reaction. The solid points are from the present work, while the open squares are the data of Häusser *et al.* (Ref. [17]).

TABLE II. Beam related analyzing power — A_{00n0}. The first uncertainty given for the present work is statistical and the second is systematic.

Beam energy	Lab angle	Present work	Häusser *et al.*
200 MeV	27.5°	0.541±0.004±0.005	0.586±0.013
	53.0°	-0.729±0.010±0.007	-0.715±0.019
	73.0°	-0.180±0.022±0.002	-0.234±0.031
500 MeV	24.0°	-0.013±0.012±0.001	0.017±0.015
	34.5°	0.300±0.022±0.003	0.256±0.029
	43.0°	0.361±0.025±0.004	0.402±0.024

TABLE III. Target related analyzing power — A_{000n}. The first uncertainty given for the present work is statistical and the second is systematic.

Beam energy	Lab angle	Present work	Häusser *et al.*
200 MeV	27.5°	0.160±0.007±0.008	0.257±0.019
	53.0°	-0.184±0.018±0.009	-0.282±0.029
	73.0°	-0.387±0.035±0.019	-0.460±0.049
500 MeV	24.0°	0.277±0.019±0.014	0.283±0.021
	34.5°	0.045±0.037±0.002	0.052±0.040
	43.0°	0.273±0.043±0.014	0.240±0.036

al., which contain no adjustable parameters. The observable A_{000n} differs significantly from the beam related observable A_{00n0} which is unambiguous evidence of a large f amplitude in the p-^{3}He t matrix even though this amplitude must vanish for the N-N system. Agreement between theory and experiment is poor for the normal observables A_{000n} and A_{00nn}. These observables are sensitive to parts of the p-^{3}He scattering amplitude untested by previous experiments. While the relativistic calculation of Ray *et al.* in general improves the agreement between theory and experiment at 500 MeV, this is likely the result of the phenomenological adjustment of some of the relevant p-^{3}He scattering amplitudes.

Absolute cross sections and the spin observables A_{00mm}, A_{00ll}, A_{00ml}, and A_{00lm} for the $^3\vec{\text{He}}(\vec{p},p)$ process have been measured at incident energies of 200 and 500 MeV. The measured differential cross sections are shown in Figs. 6 and 7 and are in good agreement with the data of Häusser *et al.* [18] and Hasell *et al.* [19]. The good agreement with the Hasell data is encouraging since in that experiment a liquid target which was 100 times thicker than the target described above was used. The theoretical calculations of Landau *et al.* [7] are in reasonable agreement with the data at 500 MeV, but at 200 MeV are larger than the data by at least an order of magnitude. This is somewhat expected in light of the fact that the impulse approximation assumed in the calculations should be more valid at the higher energy.

The normal observables measured in this experiment are shown in Fig. 8 and tabulated in Tables II, III, and IV along with the corresponding data of Häusser *et al.* The agreement with the previously measured data is reason-

TABLE IV. Spin correlation parameter — A_{00nn}.The first uncertainty given for the present work is statistical and the second is systematic.

Beam energy	Lab angle	Present work	Häusser *et al.*
200 MeV	27.5°	0.235±0.009±0.012	0.346±0.029
	53.0°	0.238±0.023±0.012	0.302±0.043
	73.0°	-0.108±0.042±0.006	-0.232±0.077
500 MeV	24.0°	0.024±0.027±0.001	0.021±0.038
	34.5°	-0.349±0.051±0.018	-0.318±0.074
	43.0°	-0.348±0.059±0.018	-0.379±0.061

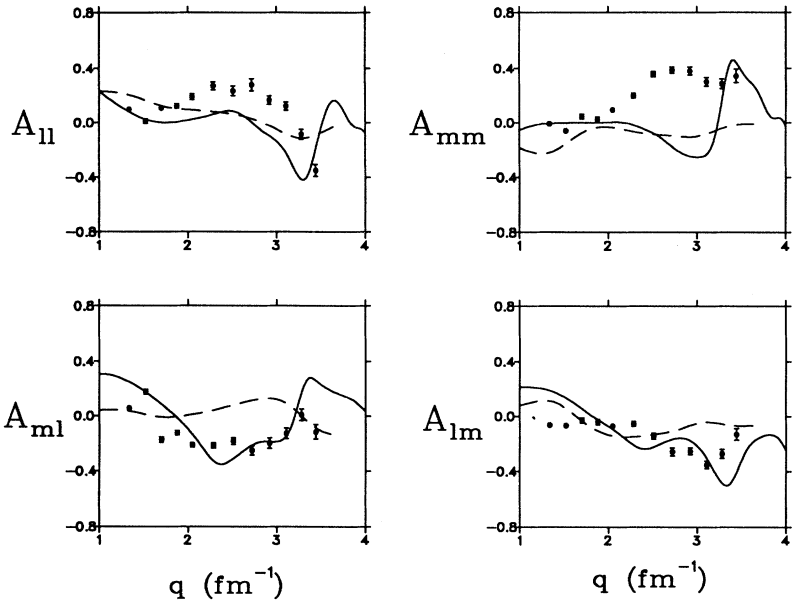

FIG. 9. In-scattering-plane spin observables for the $^3\vec{\mathrm{He}}(\vec{p},p)$ reaction at 200 MeV. The solid line is the fully microscopic optical potential calculation of Ref. [7]. The dashed line is the DWBA calculation of Ref. [8].

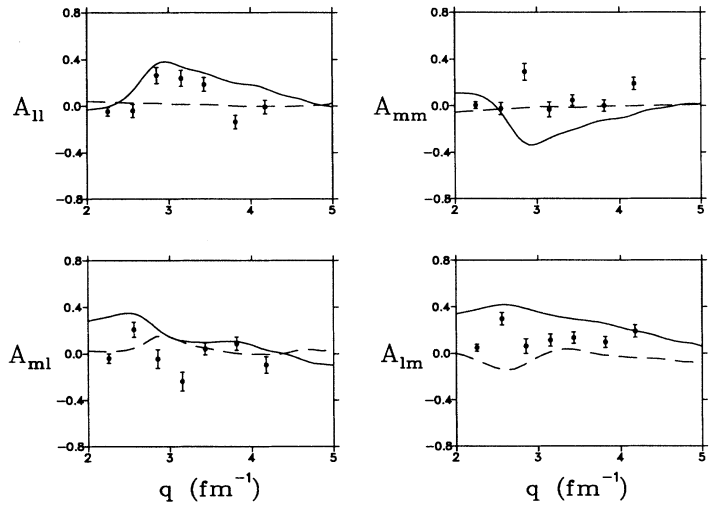

FIG. 10. In-scattering-plane spin observables for the $^3\vec{\mathrm{He}}(\vec{p},p)$ reaction at 500 MeV. The solid line is the fully microscopic optical potential calculation of Ref. [7]. The dashed line is the DWBA calculation of Ref. [8].

TABLE V. In-scattering-plane Observables for the $^3\vec{\mathrm{He}}(\vec{p},p)$ reaction at 200 MeV. The first uncertainty given is statistical and the second is systematic.

Lab angle	A_{ll}	A_{mm}	A_{ml}	A_{lm}
24.0	0.096±0.014±0.005	-0.007±0.012±0.001	-0.048±0.015±0.003	-0.071±0.015±0.003
27.5	0.021±0.017±0.001	-0.069±0.013±0.003	-0.169±0.017±0.003	-0.074±0.015±0.009
31.0	0.086±0.016±0.005	0.067±0.017±0.002	-0.177±0.016±0.002	-0.034±0.020±0.009
34.5	0.102±0.017±0.006	0.042±0.020±0.001	-0.131±0.017±0.002	-0.050±0.019±0.006
38.0	0.154±0.020±0.010	0.130±0.014±0.005	-0.219±0.017±0.004	-0.078±0.014±0.011
43.0	0.233±0.027±0.014	0.233±0.019±0.010	-0.220±0.022±0.003	-0.059±0.020±0.011
48.0	0.188±0.033±0.012	0.400±0.021±0.018	-0.159±0.025±0.007	-0.118±0.024±0.009
53.0	0.202±0.039±0.014	0.460±0.028±0.020	-0.223±0.034±0.013	-0.230±0.031±0.013
58.0	0.098±0.032±0.009	0.446±0.031±0.019	-0.152±0.035±0.013	-0.208±0.029±0.010
63.0	0.046±0.033±0.006	0.374±0.032±0.015	-0.084±0.034±0.014	-0.309±0.031±0.007
68.0	-0.120±0.037±0.005	0.319±0.036±0.014	0.082±0.037±0.018	-0.200±0.036±0.001
73.0	-0.371±0.048±0.018	0.363±0.047±0.017	0.016±0.046±0.007	0.001±0.048±0.006

TABLE VI. In-scattering-plane observables for the $^3\vec{\text{He}}(\vec{p},p)$ reaction at 500 MeV. The first uncertainty given is statistical and the second is systematic.

Lab angle	A_{ll}	A_{mm}	A_{ml}	A_{lm}
24.0	-0.046±0.037±0.003	0.003±0.029±0.001	-0.035±0.040±0.003	0.053±0.032±0.002
27.5	0.012±0.057±0.002	-0.078±0.052±0.001	0.203±0.062±0.015	0.293±0.053±0.010
31.0	0.253±0.069±0.012	0.288±0.072±0.015	-0.041±0.078±0.003	0.065±0.064±0.002
34.5	0.217±0.070±0.012	-0.013±0.064±0.002	-0.270±0.079±0.006	0.081±0.056±0.002
38.0	0.207±0.057±0.009	0.025±0.048±0.003	0.018±0.053±0.007	0.111±0.050±0.002
43.0	-0.105±0.056±0.007	-0.030±0.049±0.001	0.102±0.056±0.005	0.111±0.050±0.004
48.0	0.012±0.059±0.001	0.168±0.056±0.015	-0.066±0.065±0.010	0.220±0.054±0.005

ably good for the beam-related analyzing power, A_{n0}, at both energies and for both target-related observables at 500 MeV. The discrepancies at 200 MeV for the target-related observables are somewhat expected in light of the fact that at the lower energy, higher rates in the front-end chambers of the spectrometer lead to larger dead time and wire chamber inefficiency corrections, which could lead to larger systematic uncertainties in the spin observables than are quoted in the tables.

The in-scattering-plane spin observables are shown in Figs. 9 and 10 and are tabulated in Tables V and VI. The overall agreement between the theory and data is poor, and along with the data of Häusser *et al.* for the normal observables A_{000n}, and A_{00nn} indicates a general failure of the optical model calculations. Qualitatively, the in-scattering-plane observables are small at most momentum transfers, and especially at 500 MeV, which indicates that the amplitudes are interfering destructively. It is precisely for this reason that these data provide such a sensitive test of the current microscopic optical model reaction theories. The calculations indeed predict small observables, especially at 500 MeV, and are qualitatively consistent with the data in this regard, but with respect to the momentum dependence of the observables, the calculations bear little resemblance to the data.

At 200 and 500 MeV, there currently exist statistically reliable data for seven spin observables as well as the differential cross section over a fairly wide range of momentum transfers. The six complex amplitudes in the theory involve eleven independent parameters corresponding to the magnitude and relative phase of the six amplitudes. It may be possible, with further experimental work, to expand the spin observable data base to include spin transfer coefficients as well as some of the so-called final channel spin correlation parameters, both of which involve the measurement of the polarization of the elastically scattered proton. This is currently possible, although difficult, using the focal plane polarimeter of the MRS. If these observables were measured with a similiar statistical accuracy as the current data, then one could reliably extract the amplitudes and phases of the various amplitudes, and a comparison with the calculations at this level might help isolate the shortcomings of the theory.

Upon examination of the available experimental data for differential cross sections and spin observables for the elastic scattering reaction considered, it is seen that while the current theoretical predictions describe the differential cross section and analyzing power data quite well, all models seem to have great difficulty predicting many of the target-related and spin correlation observables. As mentioned in the Introduction, these target-spin dependent parameters provide the most severe test of the theoretical models due to their sensitivity to small changes in both the spin dependent parts of the target wave function as well as in the N-N interaction. The general disagreement observed is indicative of a lack of completeness in the models, and not of any fundamental flaw in the assumptions made in any particular model. An examination of spin observable data in other p-(few body) scattering reactions is supportive of this conclusion. For example, theoretical predictions of target-related spin observables in elastic scattering of polarized protons from polarized deuterons [20,21] require the inclusion of relativistic effects and double scattering terms to bring about quantitative agreement with the existing data. As well, inclusion of a phase variation in the N-N amplitudes is required to describe the analyzing power in the scattering of polarized protons from ^{4}He [22]. The data presented in this paper place the spin observables for the p-^{3}He system on firm experimental ground, and will hopefully provide an impetus for more sophisticated theoretical models to be considered.

ACKNOWLEDGMENTS

This work was supported by grants from the Natural Sciences and Engineering Research Council of Canada.

[1] J. Bystricky and F. Lehar, *Nucleon-Nucleon Scattering Data*, Phys. Data 11-1-11-3 (1978-1982).
[2] W. Tornow, H. Witala, and W. Glöckle, Few Body Syst. **13**, 11 (1992).
[3] M. Clajus *et al.*, Phys. Lett. B **245**, 333 (1990).
[4] B. Larson *et al.*, Phys. Rev. Lett. **67**, 3356 (1991).
[5] Yi-Fen Yen *et al.*, Phys. Rev. Lett. **66**, 1959 (1991).
[6] R. Tacik *et al.*, Phys. Rev. Lett. **63**, 1784 (1989).

[7] M.J. Paez and R.H. Landau, Phys. Rev. C **29**, 2267 (1984); R.H. Landau, M. Sagen, and G. He, Phys. Rev. C **41**, 50 (1990).
[8] L. Ray and G.W. Hoffmann, Phys. Rev. C **31**, 538 (1985). L. Ray, G.W. Hoffmann, M.L. Barlett, J.D. Lumpe, B.C. Clark, S. Hama, and R.L. Mercer, Phys. Rev. C **37**, 1169 (1988).
[9] J. Bystricky, F. Lehar, and P. Winternitz, J. Phys. (Paris) **39**, 1 (1978).
[10] P. La France and P. Winternitz, J. Phys. (Paris) **41**, 1391 (1980).
[11] G.G. Ohlsen, Rep. Prog. Phys. **35**, 717 (1972).
[12] E. Hadjimichael, B. Goulard, and R. Bornais, Phys. Rev. C **27**, 831 (1983).
[13] K.H. Hicks, TRIUMF MRS Manual (1986) (unpublished).
[14] B. Larson, O. Häusser, P.P.J. Delheij, D.M. Whittal, and D. Thiessen, Phys. Rev. A **44**, 3108 (1991).
[15] W.J. Cummings *et al.*, Nucl. Instrum. Methods A **346**, 52 (1994).
[16] O. Häusser *et al.*, TRIUMF Annual Report E616 (1991) (unpublished), p. 117.
[17] F. James and M. Roos, Comput. Phys. Commun. **10**, 343 (1975).
[18] O. Häusser *et al.*, Phys. Lett. B **343**, 36 (1995).
[19] D.K. Hasell *et al.*, Phys. Rev. C **34**, 236 (1986).
[20] D.L. Adams *et al.*, Nucl. Phys. A **480**, 530 (1980).
[21] M. Haji-Saied *et al.*, Phys. Rev. C **36**, 2010 (1987).
[22] R.J. Lombard and J.P. Maillet, Phys. Rev. C **41**, 1348 (1990).